1 Surface-enhanced Raman spectroscopy enabled evaluation

2 of bacterial inactivation



Abstract: An improved understanding of bacterial inactivation mechanisms will provide useful insights for infectious disease control and prevention. We evaluated bacterial response to several inactivation methods using surface-enhanced Raman spectroscopy (SERS). The results indicate that changes in the SERS signal are highly related to cellular disruption and cellular changes arising after cell inactivation cannot be ignored. The membrane integrity of heat and the combination of UV_{254} and free chlorine (UV_{254} /chlorine) treated *Pseudomonas syringae* (*P*. syringae) cells were severely disrupted, leading to significantly increased peak intensities. Conversely, ethanol treated bacteria exhibited intact cell morphologies and the SERS spectra remained virtually unchanged. On the basis of time dependent SERS signals, we extracted dominant SERS patterns. Peaks related to nucleic acids accounted for the main changes observed during heat, UV254, and UV254/chlorine treatment, likely due to their outward diffusion from the cell cytoplasm. For free chlorine treated P. syringae, carbohydrates and proteins on the cell membrane were denatured or lost, resulting in a decrease in related peak intensities. The nucleobases were likely oxidized when treated with UV₂₅₄ and chlorine, thus leading to shifts in the related peaks. The generality of the method was verified using two additional bacterial strains: Escherichia coli and Bacillus subtilis as well as in different water matrices. The results suggest that SERS spectral analysis is a promising means to examine bacterial stress response at the molecular level and has applicability in diverse environmental implementations.

32

33

13

14

15

16

17

18

19

20

21

22

23

24

25

26

27

28

29

30

31

Keywords: surface-enhanced Raman spectroscopy, bacteria, inactivation, multivariate analysis, water

35

1. Introduction

36

37

38

39

40

41

42

43

44

45

46

47

48

49

50

51

52

53

54

55

56

57

58

59

60

Bacterial infection is one of the leading causes of human morbidity and mortality. Pathogenic bacteria can interact with adult stem cells and manipulate or disturb cell functions and may lead to dysregulated tissue growth and the development of cancers (O'Rourke and Kempf 2019). Bacteria can be transmitted through the water supply system and the food chain. As such, various strategies have been used to control bacterial proliferation. For example, disinfection (e.g., chlorination, UV irradiation, ozonation) is a critical process for both wastewater and drinking water treatment(Crittenden et al. 2012) and sterilization (e.g., steam autoclave, dryheat sterilization) is considered an effective pretreatment technique for food preservation(Li and Farid 2016). When exposed to these severe conditions, bacterial cells as well as other microorganisms are expected to be inactivated, thus leading to a safer and heathier food and water supply. Knowledge of bacterial response to specific inactivation methods may provide useful insights that could improve the design of current methods or select the best process for a given scenario. Researchers have proposed comprehensive bacterial inactivation mechanisms, including cell membrane disruption, DNA/RNA damage, ribosome degradation, protein denaturation, etc.(Michael-Kordatou et al. 2018, Zhang et al. 2020). It is well recognized that for any specific method, all of the proposed inactivation mechanisms have the potential to be involved, thus giving rise to synergetic effects(Zhang et al. 2020). Consequently, to figure out the underlying mechanisms, a number of different analytical tools have been employed. Traditional culture-based techniques, such as plate counting and optical density measurements, are often used to assess bacterial cell viability(<u>Beal et al. 2020</u>). Whereas cell integrity can be observed through microscopy-based methods. At the molecular level, quantitative polymerase chain reaction (qPCR) or next generation sequencing (NGS) are used to monitor genome integrity while quantitative protein mass spectrometry is often employed for protein quantification(<u>Al-Jassim et al. 2017</u>, <u>Ding et al. 2019</u>, <u>Wigginton et al. 2012</u>). The combination of these strategies enables broad understanding of bacterial inactivation, but requires laborintensive pretreatment work.

61

62

63

64

65

66

67

68

69

70

71

72

73

74

75

76

77

78

79

80

81

82

83

84

85

Vibrational spectroscopic techniques have been widely used to probe biological tissues(Balan et al. 2019, Harrison and Berry 2017, Zhang et al. 2021). Spectral alterations in vibrational peaks provide rapid, nondestructive information that can be used to investigate bacterial response to stress stimuli at a molecular level. For example, Hlaing et al. utilized Fourier transform infrared spectroscopy (FTIR) to evaluate bacterial cellular component (i.e., protein, lipid, DNA, and fatty acid content) changes following drying(Hlaing et al. 2017). Raman spectroscopic changes have also been successfully employed to investigate cellular response to diverse types of oxidative stress, chemicals, and nutrients(Escoriza et al. 2007, Li et al. 2020, Malyshev et al. 2021). However, the weak signal intensity of these techniques often hinders their application. Surface-enhanced Raman spectroscopy (SERS), which takes advantage of intrinsic Raman information, but with a much higher intensity due to the use of plasmonic nanostructures, has been recently employed for biological sensing(Cialla-May et al. 2017, Wang et al. 2021a, Zong et al. 2018). Amplified cellular vibrational profiles are used for bacterial cell identification and the monitoring of metabolic activity (Bodelón et al. 2017, Plou et al. 2020, Prakash et al. 2019, Wang et al. 2021b). Moreover, by tracking changes in SERS output, researchers have been able to differentiate live and dead bacteria, as well as to evaluate bacterial survival following antibiotic exposure(Premasiri et al. 2017, Zhou et al. 2015). These studies collectively suggest that SERS may be a promising tool to probe bacterial stress responses. Despite such progress, however, there has to date been no study examining how SERS spectral alterations reveal bacterial inactivation mechanisms. Previous studies have focused on comparison of initial and final spectral status based on specific peaks (from labels, cells, or metabolites) as indicators following external stimuli(Gao et al. 2020, Guo et al. 2018,

Wang et al. 2015). As a consequence, the wide range of biomolecular changes and dynamics that occur during stimulus may remain undiscovered.

In this study, we monitored SERS spectral alterations to evaluate molecular level response of bacteria to different inactivation methods. We hypothesized that the bacterial structural and biochemical changes caused by different methods can be readily reflected by SERS signals. In this effort, *Pseudomonas syringae* was treated using five inactivation methods. Following treatment, the SERS spectra were recorded, and we applied multivariate analysis to identify the major patterns in the SERS spectra. Molecular level mechanisms were revealed by aligning the spectral variations to cellular components. Two additional bacterial strains, *Escherichia coli* and *Bacillus subtilis*, were treated similarly to verify our hypothesis that different bacteria might exhibit similar SERS responses to a given inactivation method. The results provide new insight and confirmation of bacterial inactivation mechanisms, with shorter time and less labor.

2. Materials and methods

2.1 Bacterial sample preparation

Gram-negative bacterial stains P. syringae pv phaseolicola and E. coli K12, and Gram-positive B. subtilis ATCC6051 were used as targets throughout the study. The detailed cultivation processes are listed in the Supporting Information. The obtained bacterial suspensions were washed with $1 \times$ phosphate buffered saline (PBS, Invitrogen) three times at $1753 \times g$ for 15 min. The concentration of the bacterial suspensions was obtained by counting colony forming units (CFU) and was maintained at $\sim 10^9$ CFU/mL for further proof of concept analysis. To evaluate the effect of the water matrix, $\sim 10^9$ CFU/mL of P. syringae was spiked into tap water and wastewater samples — which were collected from the Virginia Tech campus and the influent to a wastewater treatment plant in the Hampton Roads Sanitation District (HRSD; Virginia Beach, VA), respectively. Prior to use, tap water was boiled for 15 min to remove residual chlorine.

2.2 SERS measurement

111

112

113

114

115

116

117

118

119

120

121

122

123

124

125

126

127

128

129

130

131

133

134

135

SERS spectra were recorded following our previously developed method based on Concanavalin A modified bacterial cellulose nanocrystal (BCNC) decorated with AuNPs. This method has the capacity to collect bacterial fingerprint spectra with a limit of detection of approximately 1.5×10³ CFU/mL (Rahman et al. 2022). Briefly, 100 µL of PBS washed bacterial suspension was mixed with 500 µL of Concanavalin A functionalized BCNC and agitated for 1 h. Concanavalin A is a legume sourced lectin, which has high affinity to carbohydrate constituents on the bacterial surface (Kearns et al. 2017). The BCNC/bacteria mixture was centrifuged at 8720 ×g for 1 min and redispersed in a 200 µL aliquot of AuNPs. The AuNPs preparation process is listed in the Supporting Information. The negatively charged AuNPs can be easily immobilized onto the positively charged BCNC substrate (Rahman et al. 2022). The After mixing for another 5 min, the BCNC/bacteria/AuNP mixture was concentrated in 20 µL of DI water. A 5 µL aliquot of concentrated BCNC/bacteria/AuNP mixture or treated samples was pipetted onto an aluminum foil coated glass slide and air dried in a fume hood. Raman spectra were recorded using a WITec alpha500R Raman spectrometer (WITec GmbH, Ulm, Germany, spectral resolution=~3.5 cm⁻¹) with a 785 nm laser and a 10× confocal microscope objective. The signal was collected using a Peltier cooled charge coupled device with a 300 grooves per mm grating. For each sample, 100 spectra (10×10 , $X\times Y$) were acquired across a $50\times50~\mu m^2$ area with an on sample laser power of 3 mW and an integration time of 1 s for each point. A silicon wafer was used for instrumental calibration before measurement. 2.3 Bacterial inactivation and characterization

132

Five inactivation methods including common and emerging disinfection strategies (i.e., heat treatment, UV₂₅₄ treatment, ethanol treatment, free chlorine treatment, and combined UV₂₅₄ and chlorine treatment) were tested. The BCNC/bacteria/AuNP mixture was treated to monitor the signal changes arising from the bacterial cells as well as potentially released biomolecules. A 20 µL aliquot of the abovementioned concentrated mixture was heated to 100 °C in a water bath or exposed to UV light with an intensity of 10 mW/cm² for heat and UV₂₅₄ treatment, respectively. All the samples were exposed to UV₂₅₄ for 0, 10, 20, 40, and 60 min, which corresponds to UV₂₅₄ fluences of 0, 6, 12, 24, and 36 J/cm². For ethanol and free chlorine treatments, 200 µL of BCNC/bacteria/AuNP mixture was centrifuged and redispersed in 20 µL of 100% ethanol or 10 mM sodium hypochlorite (NaOCl), respectively. For UV₂₅₄/chlorine treatment, 20 µL of BCNC/bacteria/AuNP in 10 mM NaOCl was exposed to 10 mW/cm² UV₂₅₄ light. The high UV₂₅₄ and chlorine doses in the experiment were used to ensure all of the bacterial cells were inactivated. All the samples were treated for 1 h. 20 µL of BCNC/bacteria/AuNP mixture in DI water without any treatment was put in the room temperature for 1 h as a control. The relative viability, the ratio of bacterial CFU after each treatment to its initial CFU, was used to reflect the bacterial inactivation effect. Scanning electron microscope (SEM) images were collected for visualization of cellular morphology. 2.4 SERS data analysis Prior to multivariate analysis, all of the spectral data were pre-processed by instrument embedded software (Project Five) for cosmic ray removal, Savitzky-Golay smoothing, and baseline subtraction. Subsequently, the SERS data were normalized by a localized intrinsic internal standard, the pseudo peak at \sim 77 cm⁻¹ (I_{77}), which reflects the surface-enhanced elastic scattering signal, to minimize variation arising from the spatial variability of the SERS hot spots (Wei et al. 2018). This normalization method has been previously applied for a wide range of applications (Nam et al. 2020, Wang et al. 2021b). The time-dependent bacterial SERS spectra for each treatment were subjected to principal component analysis (PCA) using MATLAB® 2020b. A total of 339 Raman wavenumbers from 450 to 1700 cm⁻¹ were chosen

136

137

138

139

140

141

142

143

144

145

146

147

148

149

150

151

152

153

154

155

156

157

158

159

160

as variables. Two principal components, PC1 and PC2, were selected to best capture the

characteristics of the Raman spectra. PC loadings were performed for multiple sets of the time-dependent SERS spectra data to obtain the dominant variables. The statistical significance of these changes in the dominant peak intensities during each treatment was assessed by one-way analysis of variance (ANOVA) with Tukey's test. To provide enhanced visualization, we converted each PC1 loading plot to a SERS barcode. Such barcodes have recently been proposed as a tool to succinctly illustrate the relative intensities of all peaks in collected Raman spectra (Luo et al. 2019, Wei and Vikesland 2015). The positively contributed wavenumbers in PC1 are blue in the barcodes, while the negatively contributed wavenumbers in PC1 are in red. The color intensity reflects the PC contributions. Finally, hierarchical clustering analysis (HCA) was employed to explore the similarity and discrepancy arising from the different inactivation methods.

3. Results and discussion

3.1 Biochemical origins of P. syringae SERS spectra

We first examined the SERS spectra of freshly prepared *P. syringae* in PBS. In our method, pre-decorated concanavalin A recognizes and binds to carbohydrate constituents (e.g., glucosyl groups) expressed on the bacterial surface(Kearns et al. 2017, Rahman et al. 2022), thus enhancing the attachment of the bacteria to BCNC substrate. Subsequently added AuNPs aggregate on the bacterial surface upon droplet evaporation (Fig. 1A). Compared with bare bacterial cells, the mixture of BCNC/bacteria is expected to enhance AuNP aggregation and generate dense SERS hot spots (Fig. S1A). After forming the BCNC/bacteria/AuNP structure, we observed several distinct peaks in the region between 450 to 1700 cm⁻¹ in the SERS spectra of *P. syringae* (Fig. 1B). Well resolved and intense SERS peaks at 488, 650, 733, 997, 1023, 1240, 1312, 1467, and 1568 cm⁻¹ were observed and correspond well with the prior literature(Cui et al. 2019, Ho et al. 2019, Prakash et al. 2019, Premasiri et al. 2016, Zhou et al.

2014). The peaks of BCNC/bacteria/AuNP appear at the same positions as those for bacteria/AuNPs but with much higher intensities (Fig. S1B). This result indicates that BCNC improves the bacterial SERS intensity without resulting any changes in the measured spectral features. Besides, the coefficient of variation of the normalized intensity at 733 cm⁻¹ is 14.9% for an area scan, a value comparable to those of other bacterial detection methods(Ciloglu et al. 2020, Liu et al. 2017), thus indicating the uniformity of the acquired SERS signals (Fig. S1C). The peaks at 650 (ring breathing of guanine)(Cui et al. 2019), 733 (ring breathing of adenine) (Cui et al. 2019), 1312 (guanine)(Talari et al. 2015), and 1568 cm⁻¹ (adenine or guanine)(Kamińska et al. 2016) are contributed by nucleobases. The peaks at 997 and 1023 cm⁻¹ are assigned to the symmetric ring breathing mode and in-plane C-H bending mode of phenylalanine, respectively(Fan et al. 2011). The peak at 1240 cm⁻¹ is assigned to amide III(Cui et al. 2019). These latter peaks collectively originate from protein components. The peaks at 488 and 1467 cm⁻¹ result from polysaccharides and saturated lipids, respectively(Dina et al. 2017, Talari et al. 2015). Some minor peaks are also observed in the spectra. The detailed assignments and potential biochemical origins of all the peaks are summarized in **Table S1**. Alternative assignments have been proposed for some peaks in previous reports. For instance, some researchers have suggested that the peak at ~730 cm⁻¹ is contributed by the vibrational glycosidic ring mode of N-acetylglucosamine and the peak at \sim 650 cm⁻¹ should be assigned to phenylalanine (bending of COO⁻)(Prakash et al. 2019). Such differences can be attributed to variations in the binding affinity of the molecules to different SERS substrates and the fact that similar functional groups are present in different bacterial constituents. In the absence of P. syringae, the BCNC/AuNP substrate exhibits several minor SERS peaks. Some of the peak positions (488, 997, and 1568 cm⁻¹) are consistent with peaks also present in the *P. syringae* SERS spectra. BCNC is a bacterial by-product that contains abundant polysaccharides, proteins, and carbohydrates(Singhsa et al. 2017). These original ingredients result in the appearance of

186

187

188

189

190

191

192

193

194

195

196

197

198

199

200

201

202

203

204

205

206

207

208

209

such SERS peaks. Fortunately, however, because the peak intensities of BCNC are much weaker than those arising from the bacteria, BCNC can still be considered an excellent SERS substrate for bacterial detection.

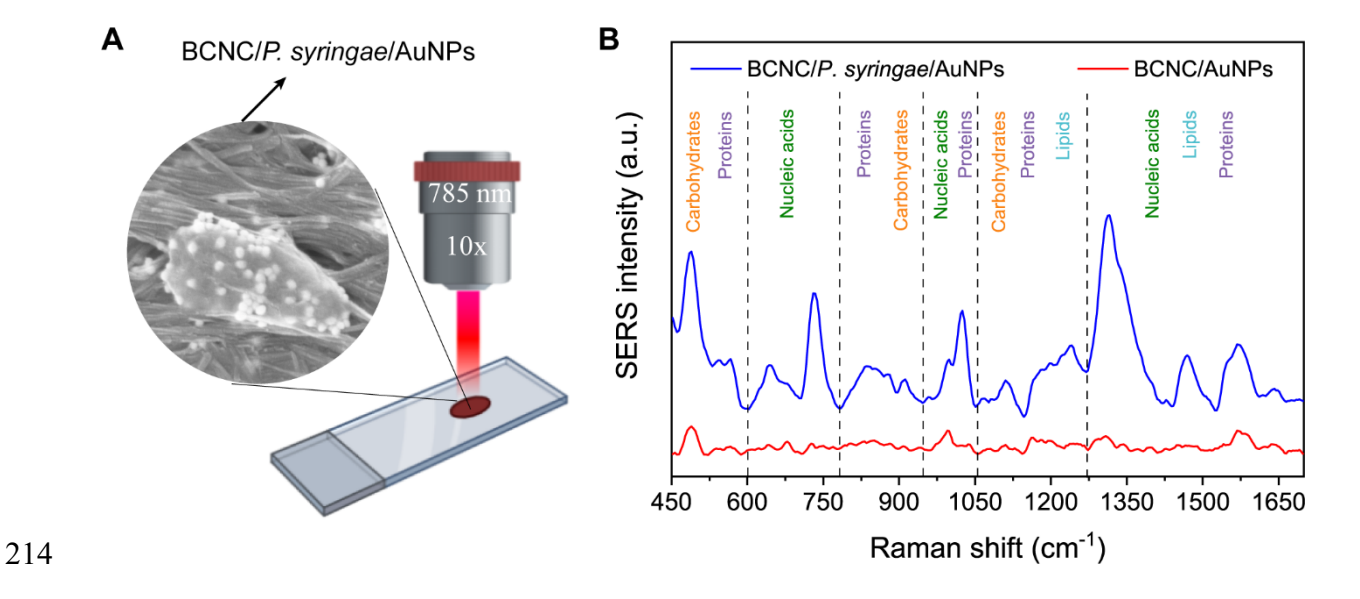


Fig. 1. (A) Schematic illustration of SERS spectra collection for *P. syringae*; the inset panel shows a SEM image of *P. syringae* on the substrate; (B) Average SERS spectra of *P. syringae* and blank substrate in the range from 450 to 1700 cm⁻¹.

3.2 SERS spectral alterations during inactivation

Instead of inactivating bacteria prior to loading the SERS substrate, we treated the combined bacteria and substrate (BCNC/bacteria/AuNP) so that we could monitor signal changes arising from the bacterial cells as well as those from molecules produced or released as a result of treatment. The first panel in **Fig. 2A** shows the SERS spectra of BCNC/P. syringae/AuNP in DI water without any additional treatment. The SERS spectra are virtually unchanged throughout the experiment thus indicating that the experimental conditions are sufficiently favorable for P. syringae to maintain viability (**Fig. 2B**). These results indicate that neither BCNC nor the AuNPs adversely influence the P. syringae cells during the measurements.

Significant spectral changes arose after treatment by each inactivation method, except for ethanol treatment (**Fig. 2**). We observed that *P. syringae* manifested notable increases in most peak regions after heat treatment, especially the peaks at 658, 733, 960, 1342, and 1455 cm⁻¹.

The peak intensities at 733 and 960 cm⁻¹ moderately increased with UV₂₅₄ radiation. Conversely, the peak intensity at 1023 cm⁻¹ decreased following UV₂₅₄ treatment. However, after being treated with ethanol, the SERS spectra remained unchanged like that of the control sample. For free chlorine treatment, the most distinct changes were observed at 488 and 674 cm⁻¹. The peak at 674 cm⁻¹ gradually increased with time, while the peak at 488 cm⁻¹ disappeared at 10 min. Unlike UV₂₅₄ alone and free chlorine alone, the SERS signals of P. syringae when confronted with UV₂₅₄/chlorine changed considerably. The peaks at 680 and 733 cm⁻¹ greatly increased with more subtle changes occurring at 960 and 1023 cm⁻¹. Despite such large spectral differences across the different inactivation methods, viability measurements for P. syringae suggest that >99% of the bacterial cells were inactivated within 10 min by all methods (**Fig. 2B**). These results indicate that the measured changes in the P. syringae SERS spectra reflect not only the inactivation process, but also the cellular changes after inactivation. Such mechanisms require further interpretation.

To ensure that the changes reflected in **Fig. 2A** primarily arise from *P. syringae*, we examined how the substrate (BCNC/AuNPs) alone was affected by each process for comparison. As shown in **Fig. S2A**, a strong peak develops at ~548 cm⁻¹ when the substrate was treated with free chlorine. Previous studies have shown that both molecular chlorine (Cl₂) and hypochlorous acid (HOCl) have Raman responses in the region of 530-560 cm⁻¹(Aggarwal et al. 2016, Cherney et al. 2006), and thus this peak reflects the presence of excess chlorinating agent in the system. We further observed this peak in our samples containing bacteria when we increased the free chlorine concentration to 50 mM (**Fig. S2B**). In addition, several minor peaks appear for BCNC after heat treatment with coincident peak positions (658, 733, and 960 cm⁻¹) to those of the bacteria samples, but with lower intensities (**Fig. S2C**). Collectively, these results indicate that SERS spectral changes arising from the substrate are minor when compared with those for the *P. syringae* samples.

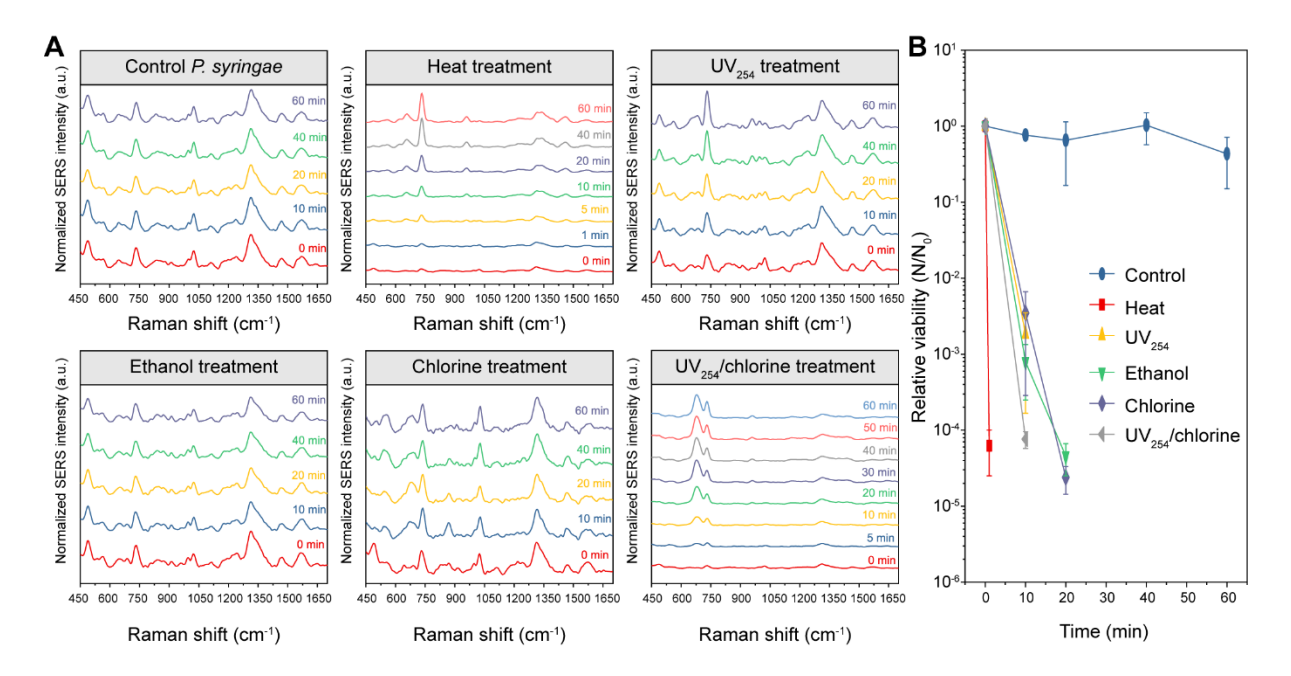


Fig. 2. (A) SERS spectra of *P. syringae* confronted with different methods as a function of time; (B) The relative viability of *P. syringae* during treatment with different methods over 60 min. The missing data points for each treatment mean no viable *P. syringae* is detected after a certain of time. The error bar reflects the standard deviation of triplicate samples.

3.3 SERS spectral based bacterial cell responses

Following our demonstration that the SERS signals of *P. syringae* can be altered during inactivation, we next evaluated biochemical changes based on the SERS spectral alterations. As mentioned previously, the SERS spectra of ethanol treated bacteria remained virtually unchanged. SEM images show that the morphology of ethanol treated *P. syringae* remained the same as the control sample (**Fig. S3**). We also collected SERS signal of *P. syringae* after treatment with different concentrations of ethanol, and the results in **Fig. S4** show that, all of the spectra remain virtually unchanged regardless of inactivation efficiency. Prior studies have established that the permeability of the cell envelope increases in the presence of ethanol due to a reduction in peptidoglycan cross-linking and the decreased lipid to protein ratio of the membrane(Dombek and Ingram 1984, Haft et al. 2014). Our SERS-based approach could not detect such changes. Therefore, we excluded ethanol treated bacteria in the following spectral analysis.

We applied PCA to identify key spectral features within the spectral range of 450 to 1700 cm⁻¹ following heat, UV₂₅₄, free chlorine, and UV₂₅₄/chlorine treatments. PCA is a linear, unsupervised visualization technique used for analyzing and reducing the dimensionality of numerical data sets in a multivariate problem(Li et al. 2018). PC loadings can be used to identify the contributions of each variable, that is the contribution of each wavenumber(Johnson et al. 2014, Shin et al. 2018). Fig. 3 presents the PC score plots of bacterial SERS spectra when exposed to different methods as a function of time. It is clearly shown that the heat, UV₂₅₄, and UV₂₅₄/chlorine processes cause the SERS spectra to be shifted to the right on the PC1 axis. A notable separation can also be seen between non-treated and treated bacteria for free chlorine treatment based solely on the PC1 score. Accordingly, we evaluated the dominant features contributing to the PC1 loading data (Fig. 4). To provide enhanced visualization, we converted each loading plot to a barcode(Luo et al. 2019, Wei and Vikesland 2015). The ten most contributing peaks were extracted from each loading plot and are listed in **Table 1**. The loading data of PC1 reveal the spectral variation contributed by the cellular components.

275

276

277

278

279

280

281

282

283

284

285

286

287

288

289

290

291292

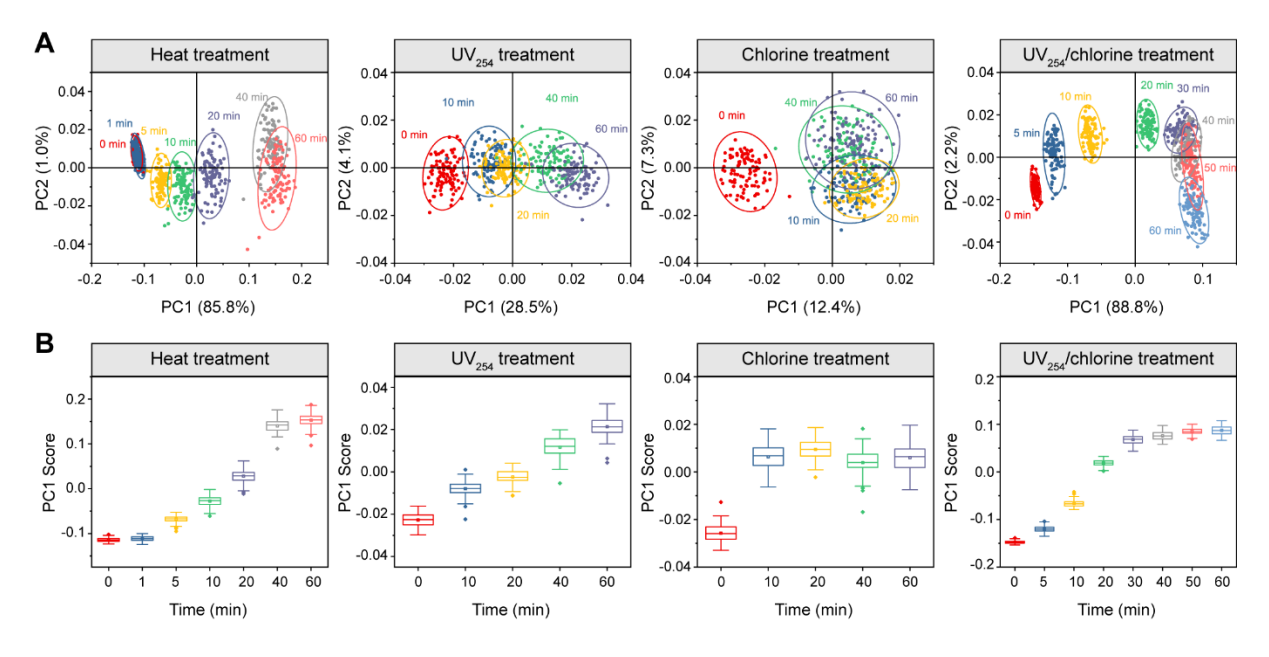


Fig. 3. (A) PCA score plots for the SERS spectra from *P. syringae* with different exposure time. The 95% confidence ellipses are illustrated.; (B) PC1 score of treated *P. syringae* under each method.

3.3.1 Heat treatment

294

295

296

297

298

299

300

301

302

303

304

305

306

307

308

309

310

311

312

313

314

315

316

317

318

Previous studies have shown that nearly all bacterial cellular components are affected when exposed to high temperatures(Cebrián et al. 2017, Russell 2003). The structures of the outer membrane, the peptidoglycan wall, and the cytoplasmic membrane are damaged, resulting in the release of lipopolysaccharides, the denaturation of proteins, and the loss of intracytoplasmic materials(Russell 2003). Ribosomes and DNA/RNA can also be damaged during heat inactivation. Fig. 4 and Table 1 reveal that each of the 10 extracted featured peaks for heat treatment positively contribute, thus implying that the intensities of all of the peaks increased with time (Fig. S5). We observed a similar increase, but with a lower peak intensity when treated at a lower temperature (80 °C) (Fig. S6). More importantly, peaks arising from nucleic acids (i.e., 658, 733, 960, 1319, 1342, and 1455 cm⁻¹) significantly contribute to PC1, followed by peaks associated with proteins (i.e., 619, 1226, 1265, and 1392 cm⁻¹). SEM images (Fig. S3) indicate that the membrane integrity of the *P. syringae* cells was severely disrupted, thus leading to completely lysed or seriously damaged cells. The increase in the intensity of all of the featured peaks possibly resulted from the release of intra-cytoplasmic nucleic acids and proteins following disruption of the highly ordered membrane structure. The increased contribution of nucleic acid related peaks following heat exposure can be attributed to the fact that purine molecules are more SERS responsive than other components (proteins, carbohydrates, or peptidoglycan constituents)(Premasiri et al. 2016). However, more advanced techniques are needed to further diagnose the metabolic source of such purine molecules.

While we successfully observed a distinctive increase in the featured peaks, some other researchers have reported different SERS/Raman spectral changes for heat treated bacteria(<u>Alula et al. 2017</u>, <u>Escoriza et al. 2007</u>, <u>Wang et al. 2010</u>, <u>Zhou et al. 2015</u>). For example, Wang et al. observed a considerable SERS signal decrease in the main spectral peaks of autoclaved *Staphylococcus aureus* and *E. coli* due to the release of carbohydrates(<u>Wang et</u>

al. 2010). Similarly, Escoriza et al. saw a decrease in normal Raman intensity for peaks around 1600 cm⁻¹ and in the region of 700 to 800 cm⁻¹ for heat treated Staphylococcus epidermidis and E. coli(Escoriza et al. 2007). They also observed the appearance of a new band at 1560 cm⁻¹ following heat treatment. Conversely, Zhou et al. found that almost no SERS signals were detected for heat killed E. coli cells(Zhou et al. 2015). Alula et al. reported that there was a blue shift in the primary peaks of heat killed *Mycobacterium tuberculosis*(Alula et al. 2017). We hypothesize that such differences in the spectra can be attributed to the discrepancy of methods. In the aforementioned studies, bacteria were usually killed in advance, and then introduced to SERS substrates. However, in our method, bacteria were mixed with the substrate prior to treatment. As such, we have the capacity to monitor signal changes arising not only from the bacterial cells, but also from biomolecules produced or released as a result of treatment. 3.3.2 UV₂₅₄ treatment It has been reported that UV light inactivates microorganisms mainly by damaging their DNA through the dimerization of thymine bases (Witkowska et al. 2019). Accordingly, SERS/Raman spectral features of nucleobases or bacteria at the region of 1300-1700 cm⁻¹ decrease(Li et al. 2019, Nagpal et al. 2021, Witkowska et al. 2019). As shown in Fig. S7, the peak at 1375 cm⁻¹ (vibrational bands of purines) slightly declines, which is consistent with the trend for UV irradiated bacteria as reported(Nagpal et al. 2021). However, 1375 cm⁻¹ was not the dominant feature altered by UV radiation herein. Instead, by tracking the 10 most contributed peaks of PC1, we found that nucleic acid related peaks (i.e., 678, 730, 960, and 1229 cm⁻¹) positively contributed, while negatively contributed peaks (i.e., 481, 823, 866, 919, 1023 cm⁻¹) reflect proteins and carbohydrates. The SEM images in Fig. S3 show that the integrity of *P. syringae* cells were slightly damaged following UV₂₅₄ treatment, leading to holes in the cell membrane. Proteins and carbohydrates on the cell membrane are expected to be denatured or lost(Kristo et al. 2012), resulting in a decrease in SERS intensity. The protein and carbohydrate peaks

319

320

321

322

323

324

325

326

327

328

329

330

331

332

333

334

335

336

337

338

339

340

341

342

declined sharply within the first 20 min and later flattened (**Fig. S8**), further illustrating that the loss of such substances occurs most likely at the cell surface. The steady increase in nucleic acid-based peaks is likely due to the outward diffusion of intracellular nucleic acids through the disrupted cell membrane. Compared with heat treated bacteria, UV_{254} treated bacteria had smaller increases in such peak intensities because of the slighter cell membrane damage. The lower the UV irradiation power intensities, the slighter the increase in SERS peak observed (**Fig. S9**). Another obvious difference displayed in the barcodes is that the featured peak at 658 cm⁻¹ for heat treatment shifted to 678 cm⁻¹ for UV_{254} treatment. This shift can be attributed to the oxidation of guanine to its derivative (8-oxoguanine) in the presence of oxidative radicals(Ibañez et al. 2015).

3.3.3 Free chlorine treatment

In contrast to heat and UV₂₅₄ treatment, the most featured peak for free chlorine treatment is negatively contributed and appears at 488 cm⁻¹ and reflects carbohydrates. Other carbohydrate/protein related peaks (835, 1215, 1240, and 1364 cm⁻¹) also declined following reaction. These results are coincident with the fact that proteins, lipids, and polysaccharides on the cell wall play significant roles in the interaction with chlorine disinfectants (Malyshev et al. 2021, Xue et al. 2013). Fig. S3 suggests that the bacterial cell membrane after free chlorine treatment was mildly affected, possibly leading to the outward diffusion of nucleic acids and a slight increase in the intensity of the purine related peaks (e.g., 674 and 741 cm⁻¹). However, such peaks exhibit a shift compared with their original position (658 and 733 cm⁻¹). Previous studies have reported that the C8 position of purine molecules can be substituted by chlorine or other halogens and results in vibrational frequency shifts. (Chen et al. 2016, Xiang et al. 2019). The shift in our work probably arises from the substitution of a chlorine atom. Another interesting trend for free chlorine treatment is that the PC1 score increased from 0 to 10 min and was then remained virtually unchanged. The high reactivity of free chlorine and the high

concentration used in our system collectively contribute to the rapid reaction kinetics for the dominant peak (488 cm⁻¹; **Figs. 2** and **S10**). We can also see from **Fig. S10** that the protein related peaks initially decreased with time that was followed by an increased period, which are possibly resulted from the initially loss of proteins on the cell membrane and the following outward diffusion of the intracellular substances, respectively.

3.3.4 UV₂₅₄/chlorine treatment

369

370

371

372

373

374

375

376

377

378

379

380

381

382

383

384

385

386

387

388

389

390

391

392

393

UV₂₅₄/chlorine can generate hydroxyl radical (·OH) and reactive chlorine species (RCS), such as Cl., ClO., and Cl₂., thus rendering it an efficient advanced oxidation process(Guo et al. 2022, Wang et al. 2020). Compared with UV₂₅₄ radiation or chlorination alone, UV₂₅₄/chlorine treated P. syringae exhibits an apparent increase in the SERS signal (Fig. 2), thus indicating that UV₂₅₄/chlorine exhibits differential inactivation performance relative to UV₂₅₄ or free chlorine alone. Table 1 and Fig. S11 show that apart from 1023 cm⁻¹, all of the other featured peaks positively contribute to PC1 with 678 and 730 cm⁻¹ being the prominent features. UV₂₅₄/chlorine treated *P. syringae* cells exhibit a roughened morphologic appearance due to the high oxidative damage of RCS compared to cells exposed to UV₂₅₄ alone or chlorine alone (Fig. S3). During UV₂₅₄/chlorine inactivation, HO· is nonselective and will be rapidly consumed while RCS selectively reacts with compounds containing electron-donating groups, such as amino acids, pyrimidines, and purines(Guo et al. 2022). The disruption of the cell membrane possibly leads to the release of intra-cytoplasmic molecules that interact with the AuNPs and results in the increase in the intensities of most peaks. Compared with other treatments, the peak of 678 cm⁻¹ contributes more. As described previously, the shift of this peak (658 to 678 cm⁻¹) arises from the oxidation of guanine. Guanine has a lower oxidation potential when compared with adenine (Ibañez et al. 2015), leading to greater increase in SERS intensity under a high oxidative condition. All these inactivation mechanisms give rise to a unique SERS barcode for UV₂₅₄/chlorine that can be easily differentiated from the other

394 treatments.

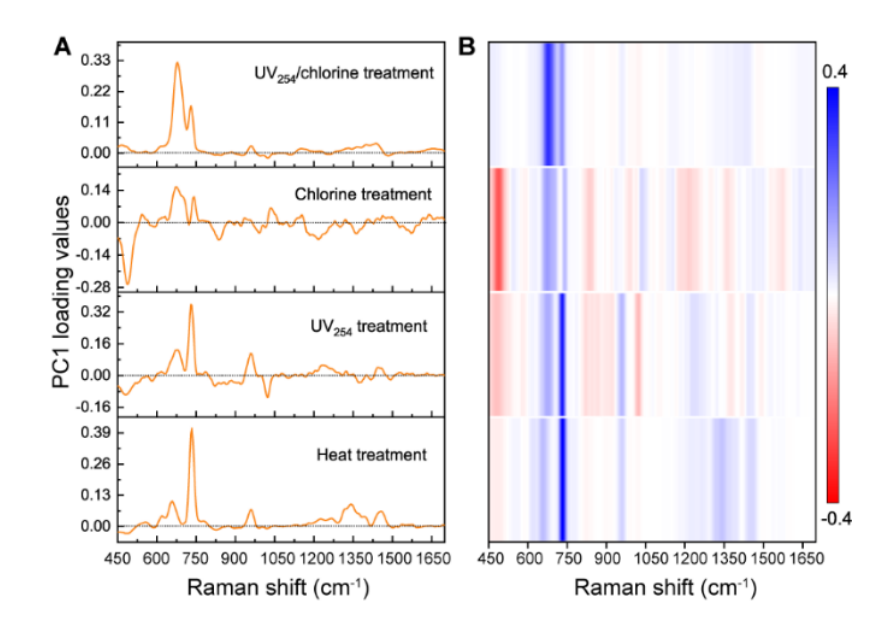


Fig. 4. (A) PC1 loading plots for the SERS spectra from *P. syringae* confronted to each method in the range from 450 to 1700 cm⁻¹; (B) the corresponding barcodes derived from loading plots.

Table 1. Top 10 contributed featured peaks extracted from PC1 loading plot after each treatment.

Peaks ^a	Contribution b	Tentative assignment	Origin	Peaks	Contribution	Tentative assignment	Origin
		Heat treatment		T T		UV ₂₅₄ treatment	
733	+	ring breathing of adenine	nucleic acids	730	+	ring breathing of adenine	nucleic acids
658	+	ring breathing of guanine	nucleic acids	678	+	ring breathing of guanine	nucleic acids
1342	+	CH2/CH3 wagging mode of guanine, adenine	nucleic acids	960	+	symmetric stretching vibration of phosphate	nucleic acids
1319	+	Guanine	nucleic acids	1023	-	the in-plane C-H bending mode of phenylalanine	proteins
960	+	symmetric stretching vibration of phosphate	nucleic acids	481	-	glycogen	carbohydrates
1455	+	deoxyribose	nucleic acids	823	-	tyrosine	proteins
619	+	C-C twisting	proteins	1229	+	antisymmetric phosphate stretching vibration	nucleic acids
1392	+	CH rocking	proteins	1237	+	amide III	proteins
1265	+	amide III	proteins	866	-	polysaccharides	carbohydrates
1226	+	amide III	proteins	919	-	C-C stretch of glucose/lactic acid	carbohydrates
		Chlorine treatment		1		UV ₂₅₄ /chlorine treatment	
488	-	glycogen	carbohydrates	678	+	ring breathing of guanine	nucleic acids
674	+	ring breathing of guanine	nucleic acids	730	+	ring breathing of adenine	nucleic acids
741	+	ring breathing of adenine	nucleic acids	1438	+	asymmetric phosphate	nucleic acids
835	-	tyrosine	proteins	1399	+	NH in-plane deformation	
1215	-	Stretching of C-N	proteins	465	+	polysaccharides	carbohydrates
1035	+	the in-plane C-H bending mode of phenylalanine	proteins	960	+	symmetric stretching vibration of phosphate	nucleic acids
1187	-	anti-symmetric phosphate vibrations	nucleic acids	619	+	C-C twisting	proteins
1240	-	amide III	proteins	1365	+	tryptophan	proteins
1364	-	tryptophan	proteins	1333	+	guanine	nucleic acids
1571	-	ring stretching of guanine, adenine	nucleic acids	1023	-	the in-plane C-H bending mode of phenylalanine	proteins

3.4 Application of SERS spectral analysis to the inactivation of other bacterial species In addition to *P. syringae*, we also investigated the SERS spectral variations of two other bacterial species: E. coli and B. subtilis. The SERS spectra and PC plots of E. coli when confronted with four inactivation methods as a function of time are illustrated in Figs. S12 and **S13**, respectively. E. coli displayed remarkable increases for most of the peaks in the regions of 450 to 1700 cm⁻¹ following heat and UV₂₅₄/chlorine treatment. In contrast, the spectral intensity changes were less obvious for cells treated with the other two methods. The results are very similar to that of P. syringae. Figs. S14 and S15 show the results for B. subtilis. Compared with P. syringae and E. coli, B. subtilis exhibited a slightly different spectral change following free chlorine treatment, especially in the region between 1200 and 1400 cm⁻¹, where proteins, carbohydrates, and nucleic acids have distinctive peaks. The differences are readily visualized in the PC1 loading barcodes in Fig. 5A and suggest a different inactivation mechanism. As a Gram-positive bacterium, B. subtilis lacks an outer membrane, but has a thicker peptidoglycan layer(Silhavy et al. 2010). In the presence of free chlorine, the highly crosslinked peptidoglycan cortex can be degraded to less-crosslinked subunits(Young and Setlow 2003). The main subunits (i.e., sugars and amino acids) are more accessible to the SERS substrate and result in higher SERS intensity. The continuous degradation of thick peptidoglycan of Gram-positive B. subtilis also led to a steady increase in the PC1 score within 60 min (Fig. S15). HCA was performed based on the PC1 loadings of all the three bacteria to further explore the similarities of the inactivation mechanisms. As demonstrated in Fig. 5B, the discriminatory SERS peaks are able to accurately cluster samples according to their respective treatment groups, except for free chlorine treated B. subtilis. In accordance with the HCA dendrogram, we can see that heat treatment and UV₂₅₄ treatment are close to each other, reflecting similar

400

401

402

403

404

405

406

407

408

409

410

411

412

413

414

415

416

417

418

419

420

421

422

423

424

inactivation mechanisms. The HCA dendrogram also shows UV₂₅₄/chlorine treatment shows

greater similarity to UV_{254} treatment than free chlorine treatment. The results collectively indicate that SERS spectral analysis is highly effective and feasible for revealing bacterial inactivation mechanisms at the biomolecular level.

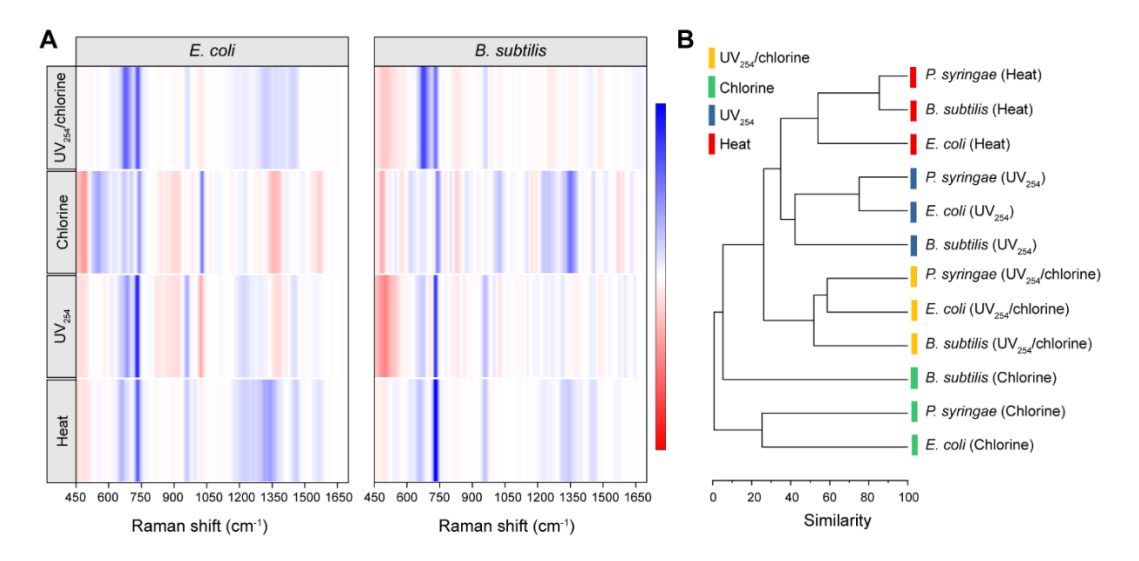
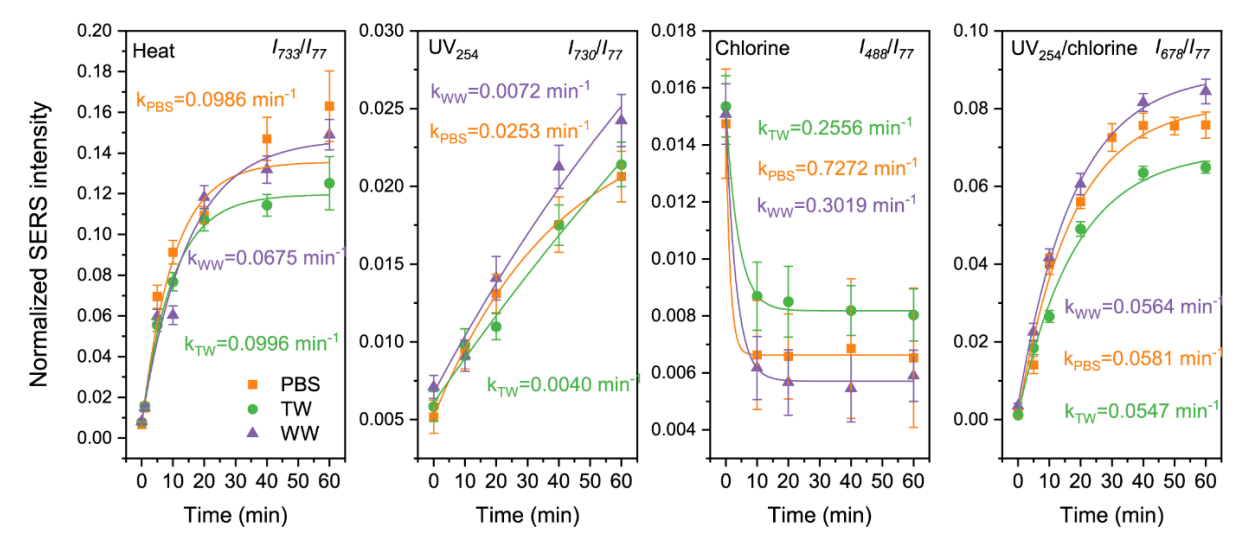


Fig. 5. (A) The barcodes derived from PC1 loading plots for *E. coli*, and *B. subtilis*. (B) dendrogram generated by HCA.

3.5 Effect of different water matrices on SERS intensity

The utility of using SERS spectral variations to monitor bacterial inactivation was tested in tap water and wastewater matrices and then compared to that in PBS. The parameters for each water sample are listed in **Table S2**. Although wastewater contained bacterial cells ($\sim 10^3$ CFU/mL), the concentration was much lower than that of the spiked *P. syringae* ($\sim 10^9$ CFU/mL) and would cause negligible effect on our results. **Fig. 6** shows the temporal variation of the normalized SERS intensity of the most contributed featured peaks for each inactivation method (i.e., I_{733}/I_{77} for heat treatment, I_{730}/I_{77} for UV₂₅₄ treatment, I_{488}/I_{77} for free chlorine treatment, and I_{678}/I_{77} for UV₂₅₄/chlorine treatment) in the different water matrices. We can see from the results that the SERS intensity alterations of *P. syringae* in both tap water and wastewater are similar to that in PBS. To have a better understanding of the reaction kinetics, a first order model was applied to fit the data. The equation is described as $I_t = I_e - Ae^{-kt}$. I_t and I_e are normalized intensity at time t and equilibrium. t is the SERS intensity change rate constant. A

is the parameter which reflects the discrepancy between final and initial intensities. A is positive when the SERS intensity increases with time (i.e., heat, UV₂₅₄, and UV₂₅₄/chlorine treatment in our case) and negative for I_{488}/I_{77} for free chlorine treatment. The fitting parameters are listed in Table S3. As revealed in Fig. 6 and Table S3, the free chlorine treatment has the highest SERS intensity change rate constant ($k=0.256\sim0.727$ min⁻¹) for all scenarios, which is consistent with our previous interpretation that the reaction for chlorine treatment mainly occurred on the cell membrane. The high reactivity of chlorine and the high concentration used in our system contribute to the rapid reaction kinetics. It is worth noting that the rate constant k determined herein reflects the intensity changes in the bacterial cellular signals and not the loss of bacterial viability. For example, heat treatment induces a more rapid decline in bacterial viability loss than free chlorine (Fig. 2B) but has a smaller rate constant for the change in SERS intensity. These results indicate that SERS signals arising from bacterial cellular components can still change even after cellular inactivation by heat treatment. Besides, k_{TW} and k_{WW} are compatible to k_{PBS} for heat and UV₂₅₄/chlorine treatments; k_{TW} and k_{WW} declined for UV₂₅₄ treatment and free chlorine treatment. As discussed previously, UV254 treatment and free chlorine treatment could cause less damage to bacterial cells than heat and UV₂₅₄/chlorine treatments, which may be more greatly affected by the organic constituents and alkalinity of such waters.



445

446

447

448

449

450

451

452

453

454

455

456

457

458

459

460

461

Fig. 6. Variation of normalized SERS intensity as a function of time when treated with different inactivation methods in PBS, tap water (TW), and wastewater (WW). The peaks used for normalization were the most contributed featured peaks in each method. The data was fitted with first order kinetic model.

4. Conclusions

The present study applied SERS to reveal bacterial cellular composition and its alterations during inactivation. With the help of multivariate analysis, we are able to identify the dominant spectral features arising from the biomarkers for each treatment. The results indicate that SERS spectral changes are highly related to cellular disruption, and consequently, the released nucleic acids dominate the spectral alterations observed for most of the treatments. The loss of carbohydrates and proteins from the cell membrane, the release of intracytoplasmic protein-related constituents, and even the oxidation of some biomolecules could be clearly detected within the time-dependent SERS results and are well reflected in the barcodes. The SERS barcodes and HCA results suggest SERS responses of different bacterial strains are in accordance with inactivation methods. When applied to real water matrices, we observe similar biochemical changes for the same treatment, but different rate constants, due to the complexity of real water samples. These results collectively suggest that SERS spectral analysis is a promising means to reveal bacterial stress responses at the molecular level and offers potential for diverse environmental implementation.

Declaration of Competing Interest

The authors declare no competing financial interest.

Acknowledgement

This research was supported by the US National Science Foundation grants OISE-1545756 and CBET-2029911. Laboratory and instrumentation support was provided by NanoEarth – a node of the NSF supported NNCI (NSF award number #2025151). Additional support was provided by the Sustainable Nanotechnology Interdisciplinary Graduate Program (VTSuN IGEP)

- 492 funded by the Virginia Tech Graduate School. We also gratefully thank HRSD for kindly
- 493 providing wastewater samples.

494 Supplementary materials

Supplementary materials associated with this article can be found, in the online version.

496

497 References

- 498 Aggarwal, R.L., Farrar, L., Di Cecca, S. and Jeys, T. 2016. Raman spectra and cross sections
- 499 of ammonia, chlorine, hydrogen sulfide, phosgene, and sulfur dioxide toxic gases in the
- 500 fingerprint region 400-1400 cm⁻¹. AIP Advances 6(2), 025310.
- Al-Jassim, N., Mantilla-Calderon, D., Wang, T. and Hong, P.-Y. 2017. Inactivation and gene
- 502 expression of a virulent wastewater *Escherichia coli* strain and the nonvirulent commensal
- 503 Escherichia coli DSM1103 strain upon solar irradiation. Environ. Sci. Technol. 51(7), 3649-
- 504 3659.
- Alula, M.T., Krishnan, S., Hendricks, N.R., Karamchand, L. and Blackburn, J.M. 2017.
- 506 Identification and quantitation of pathogenic bacteria via in-situ formation of silver
- nanoparticles on cell walls, and their detection via SERS. Microchim. Acta 184(1), 219-227.
- Balan, V., Mihai, C.-T., Cojocaru, F.-D., Uritu, C.-M., Dodi, G., Botezat, D. and Gardikiotis,
- 509 I. 2019. Vibrational spectroscopy fingerprinting in medicine: from molecular to clinical
- 510 practice. Materials 12(18), 2884.
- Beal, J., Farny, N.G., Haddock-Angelli, T., Selvarajah, V., Baldwin, G.S., Buckley-Taylor, R.,
- Gershater, M., Kiga, D., Marken, J. and Sanchania, V. 2020. Robust estimation of bacterial cell
- count from optical density. Commun. Biol. 3(1), 1-29.
- Bodelón, G., Montes-García, V., Costas, C., Pérez-Juste, I., Pérez-Juste, J., Pastoriza-Santos,
- 515 I. and Liz-Marzán, L.M. 2017. Imaging bacterial interspecies chemical interactions by surface-
- enhanced Raman scattering. ACS Nano 11(5), 4631-4640.
- 517 Cebrián, G., Condón, S. and Mañas, P. 2017. Physiology of the inactivation of vegetative
- 518 bacteria by thermal treatments: mode of action, influence of environmental factors and
- 519 inactivation kinetics. Foods 6(12), 107.
- 520 Chen, Y.-L., Wu, D.-Y. and Tian, Z.-Q. 2016. Theoretical investigation on the substituent
- effect of halogen atoms at the C8 Position of adenine: relative stability, vibrational frequencies,
- and Raman spectra of tautomers. J. Phys. Chem. A 120(23), 4049-4058.
- 523 Cherney, D.P., Duirk, S.E., Tarr, J.C. and Collette, T.W. 2006. Monitoring the speciation of

- aqueous free chlorine from pH 1 to 12 with Raman spectroscopy to determine the identity of
- 525 the potent low-pH oxidant. Appl. Spectrosc. 60(7), 764-772.
- 526 Cialla-May, D., Zheng, X.-S., Weber, K. and Popp, J. 2017. Recent progress in surface-
- enhanced Raman spectroscopy for biological and biomedical applications: from cells to clinics.
- 528 Chem. Soc. Rev. 46(13), 3945-3961.
- 529 Ciloglu, F.U., Saridag, A.M., Kilic, I.H., Tokmakci, M., Kahraman, M. and Aydin, O. 2020.
- 530 Identification of methicillin-resistant Staphylococcus aureus bacteria using surface-enhanced
- Raman spectroscopy and machine learning techniques. Analyst 145(23), 7559-7570.
- Crittenden, J.C., Trussell, R.R., Hand, D.W., Howe, K.J. and Tchobanoglous, G. 2012. MWH's
- water treatment: principles and design, John Wiley & Sons.
- Cui, L., Zhang, D., Yang, K., Zhang, X. and Zhu, Y.-G. 2019. Perspective on surface-enhanced
- Raman spectroscopic investigation of microbial world. Anal. Chem. 91(24), 15345-15354.
- Dina, N., Zhou, H., Colniță, A., Leopold, N., Szoke-Nagy, T., Coman, C. and Haisch, C. 2017.
- Rapid single-cell detection and identification of pathogens by using surface-enhanced Raman
- 538 spectroscopy. Analyst 142(10), 1782-1789.
- Ding, W., Jin, W., Cao, S., Zhou, X., Wang, C., Jiang, Q., Huang, H., Tu, R., Han, S.-F. and
- Wang, Q. 2019. Ozone disinfection of chlorine-resistant bacteria in drinking water. Water Res.
- 541 160, 339-349.
- Dombek, K.M. and Ingram, L. 1984. Effects of ethanol on the Escherichia coli plasma
- 543 membrane. J. Bacteriol. 157(1), 233-239.
- 544 Escoriza, M.F., VanBriesen, J.M., Stewart, S. and Maier, J. 2007. Raman spectroscopic
- discrimination of cell response to chemical and physical inactivation. Appl. Spectrosc. 61(8),
- 546 812-823.
- Fan, C., Hu, Z., Mustapha, A. and Lin, M. 2011. Rapid detection of food-and waterborne
- bacteria using surface-enhanced Raman spectroscopy coupled with silver nanosubstrates. Appl.
- 549 Microbiol. Biotechnol. 92(5), 1053-1061.
- Gao, X., Yin, Y., Wu, H., Hao, Z., Li, J., Wang, S. and Liu, Y. 2020. Integrated SERS platform
- for reliable detection and photothermal elimination of bacteria in whole blood samples. Anal.
- 552 Chem. 93(3), 1569-1577.
- Guo, J., Liu, Y., Chen, Y., Li, J. and Ju, H. 2018. A multifunctional SERS sticky note for real-
- 554 time quorum sensing tracing and inactivation of bacterial biofilms. Chem. Sci. 9(27), 5906-
- 555 5911.
- Guo, K., Wu, Z., Chen, C. and Fang, J. 2022. UV/Chlorine Process: An Efficient Advanced

- Oxidation Process with Multiple Radicals and Functions in Water Treatment. Acc. Chem. Res.,
- 558 1859-1868.
- Haft, R.J., Keating, D.H., Schwaegler, T., Schwalbach, M.S., Vinokur, J., Tremaine, M., Peters,
- J.M., Kotlajich, M.V., Pohlmann, E.L. and Ong, I.M. 2014. Correcting direct effects of ethanol
- on translation and transcription machinery confers ethanol tolerance in bacteria. Proc. Natl.
- 562 Acad. Sci. USA 111(25), E2576-E2585.
- Harrison, J.P. and Berry, D. 2017. Vibrational spectroscopy for imaging single microbial cells
- in complex biological samples. Front. Microbiol. 8, 675.
- Hlaing, M.M., Wood, B.R., McNaughton, D., Ying, D., Dumsday, G. and Augustin, M.A. 2017.
- 566 Effect of drying methods on protein and DNA conformation changes in Lactobacillus
- *rhamnosus* GG cells by Fourier transform infrared spectroscopy. J. Agric. Food Chem. 65(8),
- 568 1724-1731.
- Ho, C.-S., Jean, N., Hogan, C.A., Blackmon, L., Jeffrey, S.S., Holodniy, M., Banaei, N., Saleh,
- A.A., Ermon, S. and Dionne, J. 2019. Rapid identification of pathogenic bacteria using Raman
- 571 spectroscopy and deep learning. Nat. Commun. 10(1), 1-8.
- 572 Ibañez, D., Santidrian, A., Heras, A., Kalbáč, M. and Colina, A. 2015. Study of adenine and
- 573 guanine oxidation mechanism by surface-enhanced Raman spectroelectrochemistry. J. Phys.
- 574 Chem. C 119(15), 8191-8198.
- Johnson, C.M., Pleshko, N., Achary, M. and Suri, R.P. 2014. Rapid and sensitive screening of
- 576 17β-estradiol estrogenicity using Fourier transform infrared imaging spectroscopy (FT-IRIS).
- 577 Environ. Sci. Technol. 48(8), 4581-4587.
- Kamińska, A., Witkowska, E., Kowalska, A., Skoczyńska, A., Ronkiewicz, P., Szymborski, T.
- and Waluk, J. 2016. Rapid detection and identification of bacterial meningitis pathogens in ex
- vivo clinical samples by SERS method and principal component analysis. Anal. Methods 8(22),
- 581 4521-4529.
- Kearns, H., Goodacre, R., Jamieson, L.E., Graham, D. and Faulds, K. 2017. SERS detection of
- multiple antimicrobial-resistant pathogens using nanosensors. Anal. Chem. 89(23), 12666-
- 584 12673.
- Kristo, E., Hazizaj, A. and Corredig, M. 2012. Structural changes imposed on whey proteins
- by UV irradiation in a continuous UV light reactor. J. Agric. Food Chem. 60(24), 6204-6209.
- 587 Li, H., Zhang, D., Luo, J., Jones, K.C. and Martin, F.L. 2020. Applying Raman
- Microspectroscopy to Evaluate the Effects of Nutrient Cations on Alkane Bioavailability to
- Acinetobacter baylyi ADP1. Environ. Sci. Technol. 54(24), 15800–15810.

- Li, R., Dhankhar, D., Chen, J., Krishnamoorthi, A., Cesario, T.C. and Rentzepis, P.M. 2019.
- Identification of live and dead bacteria: A Raman spectroscopic study. IEEE Access 7, 23549-
- 592 23559.
- 593 Li, R., Goswami, U., King, M., Chen, J., Cesario, T.C. and Rentzepis, P.M. 2018. In situ
- detection of live-to-dead bacteria ratio after inactivation by means of synchronous fluorescence
- and PCA. Proc. Natl. Acad. Sci. USA 115(4), 668-673.
- 596 Li, X. and Farid, M. 2016. A review on recent development in non-conventional food
- sterilization technologies. J. Food Eng. 182, 33-45.
- Liu, Y., Zhou, H., Hu, Z., Yu, G., Yang, D. and Zhao, J. 2017. Label and label-free based
- 599 surface-enhanced Raman scattering for pathogen bacteria detection: A review. Biosens.
- 600 Bioelectron. 94, 131-140.
- Luo, X., Jiang, L., Kang, T., Xing, Y., Zheng, E., Wu, P., Cai, C. and Yu, Q. 2019. Label-free
- Raman observation of TET1 protein-mediated epigenetic alterations in DNA. Anal. Chem.
- 603 91(11), 7304-7312.
- Malyshev, D., Dahlberg, T., Wiklund, K., Andersson, P.O., Henriksson, S. and Andersson, M.
- 2021. Mode of Action of Disinfection Chemicals on the Bacterial Spore Structure and Their
- 606 Raman Spectra. Anal. Chem. 93(6), 3146–3153.
- Michael-Kordatou, I., Karaolia, P. and Fatta-Kassinos, D. 2018. The role of operating
- parameters and oxidative damage mechanisms of advanced chemical oxidation processes in
- 609 the combat against antibiotic-resistant bacteria and resistance genes present in urban
- 610 wastewater. Water Res. 129, 208-230.
- Nagpal, A., Dhankhar, D., Cesario, T.C., Li, R., Chen, J. and Rentzepis, P.M. 2021. Thymine
- dissociation and dimer formation: A Raman and synchronous fluorescence spectroscopic study.
- 613 Proc. Natl. Acad. Sci. USA 118(6), e2025263118.
- Nam, W., Zhao, Y., Song, J., Ali Safiabadi Tali, S., Kang, S., Zhu, W., Lezec, H.J., Agrawal,
- A., Vikesland, P.J. and Zhou, W. 2020. Plasmonic electronic raman scattering as internal
- 616 standard for spatial and temporal calibration in quantitative surface-enhanced raman
- 617 spectroscopy. J. Phys. Chem. Lett. 11(22), 9543-9551.
- O'Rourke, F. and Kempf, V.A. 2019. Interaction of bacteria and stem cells in health and disease.
- 619 FEMS Microbiol. Rev. 43(2), 162-180.
- Plou, J., García, I., Charconnet, M., Astobiza, I., García-Astrain, C., Matricardi, C., Mihi, A.,
- 621 Carracedo, A. and Liz-Marzán, L.M. 2020. Multiplex SERS Detection of Metabolic
- Alterations in Tumor Extracellular Media. Adv. Funct. Mater. 30(17), 1910335.

- Prakash, O., Sil, S., Verma, T. and Umapathy, S. 2019. Direct detection of bacteria using
- 624 positively charged Ag/Au bimetallic nanoparticles: A label-free surface-enhanced raman
- scattering study coupled with multivariate analysis. J. Phys. Chem. C 124(1), 861-869.
- 626 Premasiri, W., Chen, Y., Williamson, P., Bandarage, D., Pyles, C. and Ziegler, L. 2017. Rapid
- 627 urinary tract infection diagnostics by surface-enhanced Raman spectroscopy (SERS):
- identification and antibiotic susceptibilities. Anal. Bioanal. Chem. 409(11), 3043-3054.
- Premasiri, W.R., Lee, J.C., Sauer-Budge, A., Theberge, R., Costello, C.E. and Ziegler, L.D.
- 630 2016. The biochemical origins of the surface-enhanced Raman spectra of bacteria: a
- metabolomics profiling by SERS. Anal. Bioanal. Chem. 408(17), 4631-4647.
- Rahman, A., Kang, S., Wang, W., Huang, Q., Kim, I. and Vikesland, P.J. 2022. Lectin-
- 633 modified bacterial cellulose nanocrystals decorated with Au nanoparticles for selective
- detection of bacteria using surface-enhanced Raman scattering coupled with machine learning.
- 635 ACS Appl. Nano Mater. 5(1), 259-268.
- Russell, A. 2003. Lethal effects of heat on bacterial physiology and structure. Sci. Prog. 86(1-
- 637 2), 115-137.
- 638 Shin, H., Jeong, H., Park, J., Hong, S. and Choi, Y. 2018. Correlation between cancerous
- exosomes and protein markers based on surface-enhanced Raman spectroscopy (SERS) and
- principal component analysis (PCA). ACS Sens. 3(12), 2637-2643.
- 641 Silhavy, T.J., Kahne, D. and Walker, S. 2010. The bacterial cell envelope. Cold Spring Harb.
- 642 Perspect. Biol. 2(5), a000414.
- 643 Singhsa, P., Narain, R. and Manuspiya, H. 2017. Bacterial cellulose nanocrystals (BCNC)
- preparation and characterization from three bacterial cellulose sources and development of
- 645 functionalized BCNCs as nucleic acid delivery systems. ACS Appl. Nano Mater. 1(1), 209-
- 646 221.
- Talari, A.C.S., Movasaghi, Z., Rehman, S. and Rehman, I.U. 2015. Raman spectroscopy of
- 648 biological tissues. Appl. Spectrosc. Rev. 50(1), 46-111.
- Wang, H., Wang, J., Li, S., Ding, G., Wang, K., Zhuang, T., Huang, X. and Wang, X. 2020.
- 650 Synergistic effect of UV/chlorine in bacterial inactivation, resistance gene removal, and gene
- conjugative transfer blocking. Water Res. 185, 116290.
- 652 Wang, H., Zhou, Y., Jiang, X., Sun, B., Zhu, Y., Wang, H., Su, Y. and He, Y. 2015.
- 653 Simultaneous capture, detection, and inactivation of bacteria as enabled by a surface-enhanced
- Raman scattering multifunctional chip. Angew. Chem. 127(17), 5221-5225.
- Wang, P., Sun, Y., Li, X., Wang, L., Xu, Y., He, L. and Li, G. 2021a. Recent advances in dual

- 656 recognition based surface enhanced Raman scattering for pathogenic bacteria detection: A
- review. Anal. Chim. Acta, 338279.
- Wang, W., Kang, S. and Vikesland, P.J. 2021b. Surface-enhanced Raman spectroscopy of
- bacterial metabolites for bacterial growth monitoring and diagnosis of viral infection. Environ.
- 660 Sci. Technol. 55(13), 9119-9128.
- Wang, Y., Lee, K. and Irudayaraj, J. 2010. Silver nanosphere SERS probes for sensitive
- identification of pathogens. J. Phys. Chem. C 114(39), 16122-16128.
- Wei, H., Leng, W., Song, J., Willner, M.R., Marr, L.C., Zhou, W. and Vikesland, P.J. 2018.
- Improved quantitative SERS enabled by surface plasmon enhanced elastic light scattering.
- 665 Anal. Chem. 90(5), 3227-3237.
- Wei, H. and Vikesland, P.J. 2015. pH-triggered molecular alignment for reproducible SERS
- detection via an AuNP/nanocellulose platform. Sci. Rep. 5(1), 1-10.
- Wigginton, K.R., Pecson, B.M., Sigstam, T.r., Bosshard, F. and Kohn, T. 2012. Virus
- inactivation mechanisms: impact of disinfectants on virus function and structural integrity.
- 670 Environ. Sci. Technol. 46(21), 12069-12078.
- Witkowska, E., Niciński, K., Korsak, D., Szymborski, T. and Kamińska, A. 2019. Sources of
- variability in SERS spectra of bacteria: comprehensive analysis of interactions between
- selected bacteria and plasmonic nanostructures. Anal. Bioanal. Chem. 411(10), 2001-2017.
- Kiang, Y., Deng, Z., Yang, X., Shang, C. and Zhang, X. 2019. Transformation of adenine and
- 675 cytosine in chlorination-An ESI-tqMS investigation. Chemosphere 234, 505-512.
- Xue, Z., Hessler, C.M., Panmanee, W., Hassett, D.J. and Seo, Y. 2013. Pseudomonas
- 677 aeruginosa inactivation mechanism is affected by capsular extracellular polymeric substances
- 678 reactivity with chlorine and monochloramine. FEMS Microbiol. Ecol. 83(1), 101-111.
- Young, S. and Setlow, P. 2003. Mechanisms of killing of *Bacillus subtilis* spores by
- 680 hypochlorite and chlorine dioxide. J. Appl. Microbiol. 95(1), 54-67.
- Zhang, D., Zhang, X., Ma, R., Deng, S., Wang, X., Wang, X., Zhang, X., Huang, X., Liu, Y.,
- 682 Li, G., Qu, J., Zhu, Y. and Li, J. 2021. Ultra-fast and onsite interrogation of Severe Acute
- Respiratory Syndrome Coronavirus 2 (SARS-CoV-2) in waters via surface enhanced Raman
- 684 scattering (SERS). Water Res. 200, 117243.
- Zhang, H., Tikekar, R.V., Ding, Q., Gilbert, A.R. and Wimsatt, S.T. 2020. Inactivation of
- 686 foodborne pathogens by the synergistic combinations of food processing technologies and
- 687 food-grade compounds. Compr. Rev. Food Sci. Food Saf. 19(4), 2110-2138.
- Zhou, H., Yang, D., Ivleva, N.P., Mircescu, N.E., Niessner, R. and Haisch, C. 2014. SERS

- detection of bacteria in water by in situ coating with Ag nanoparticles. Anal. Chem. 86(3),
- 690 1525-1533.
- Zhou, H., Yang, D., Ivleva, N.P., Mircescu, N.E., Schubert, S.r., Niessner, R., Wieser, A. and
- Haisch, C. 2015. Label-free in situ discrimination of live and dead bacteria by surface-
- enhanced Raman scattering. Anal. Chem. 87(13), 6553-6561.
- 694 Zong, C., Xu, M., Xu, L.-J., Wei, T., Ma, X., Zheng, X.-S., Hu, R. and Ren, B. 2018. Surface-
- enhanced Raman spectroscopy for bioanalysis: reliability and challenges. Chem. Rev. 118(10),
- 696 4946-4980.